Chapter 7
Low Cycle Fatigue Behavior at 600 °C

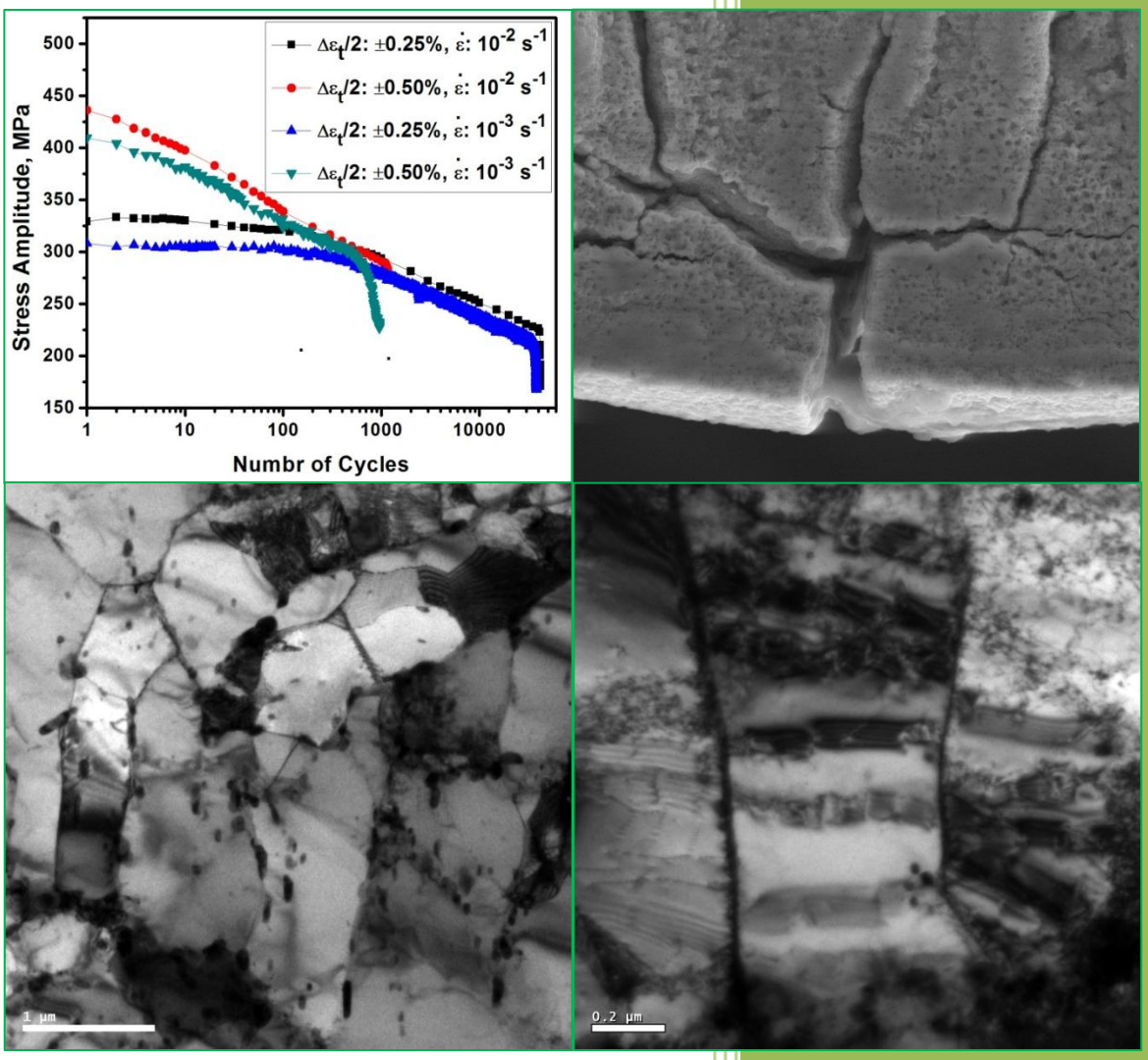

7.1 Introduction

In this chapter LCF behavior of modified 9Cr–1Mo steel in normalized & tempered condition is presented for different total strain amplitudes from ±0.25% to ±0.50% at strain rates of 10^{-2} s^{-1} & 10^{-3} s^{-1} at 600 °C. At lower strain amplitudes this steel exhibits stabilized stress response in the initial stage followed by softening till failure. However, at high strain amplitudes there is continuous softening from the first cycle till the failure. Cyclic stress response is increased with increase in strain rate from 10^{-3} s^{-1} to 10^{-2} s^{-1}, while there is lower fatigue life at the lower strain rate of 10^{-3} s^{-1}. The fracture surface is found oxidized which is assumed to play major role in reduction in life particular at the low strain rate. TEM study of the fatigue tested specimens revealed that cyclic softening is associated with many factors such as cell formation, dynamic recovery/recrystallization, grain rotation, coarsening of carbides and annihilation of the arrays of dislocations.

7.2 Cyclic Stress Response

Figure 7.1 shows the variation of cyclic stress amplitude with number of cycles of the modified 9Cr–1Mo steel in normalized and tempered condition at different total strain amplitudes from ±0.25% to ±0.50% at strain rates of 10^{-2} s^{-1} & 10^{-3} s^{-1} at 600 °C. Cyclic softening, regardless of strain amplitude may be seen. At high strain amplitudes there is continuous softening from the first cycle till failure, however, on the other hand, a stabilized stress response followed by cyclic softening at low strain amplitudes. The number of cycles corresponding to stable stress response is found to decrease with increase in strain amplitude. The extent of cyclic softening is increased with increase in strain amplitude.

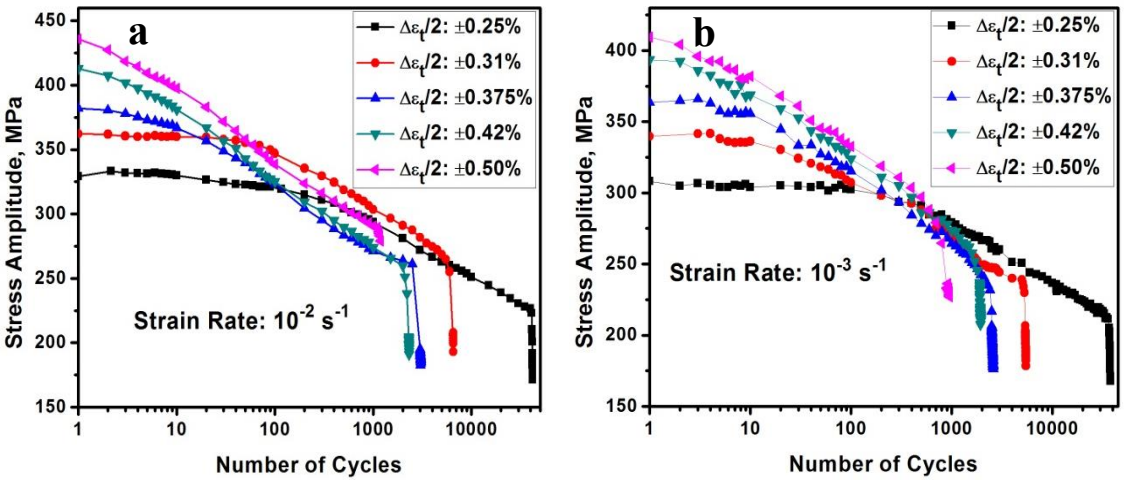

Fig. 7.1 Effect of strain amplitude on cyclic stress response of modified 9Cr–1Mo steel at different strain rates: (a) 10^{-2} s^{-1} (b) 10^{-3} s^{-1} at 600 °C.

The effect of strain rate on cyclic stress response at strain amplitudes of ±0.25% and ±0.50% is shown in Fig. 7.2. It is quite obvious from the figure that similar type of cyclic stress response is observed at both the strain rates. However, magnitude of stress amplitude for each cycle is increased with increase in strain rate, at both the strain amplitudes.

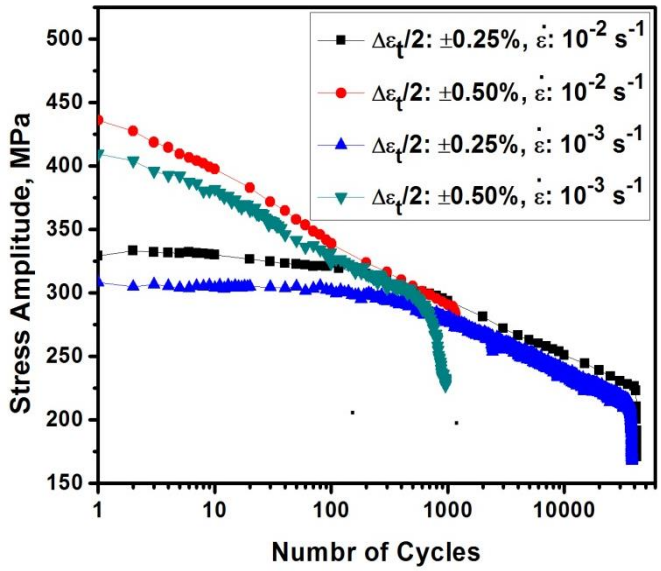

Fig.7.2 Effect of strain rate on cyclic stress response at strain amplitudes of ±0.25% & ±0.50%.

The rate of cyclic softening is also found to be same at both the strain rates at identical total strain amplitudes.

7.3 Dependence of Fatigue Life on Plastic Strain Amplitude

The number of reversals to failure ($2N_f$) as a function of plastic strain amplitude ($\Delta\varepsilon_p/2$) is plotted on log–log scale using Coffin–Manson relationship [131] given in Fig. 7.3. LCF parameters are summarized for both strain rates 10^{-2} s^{-1} and 10^{-3} s^{-1} in Table 7.1. It is obvious that fatigue ductility coefficient decreased with decrease in strain rate. There is abnormal trend in the variation of fatigue life with strain amplitude. In general fatigue life increases with increase in strain rate. However, fatigue life is decreased with decrease in strain rate from 10^{-2} s^{-1} to 10^{-3} s^{-1} at 600 °C.

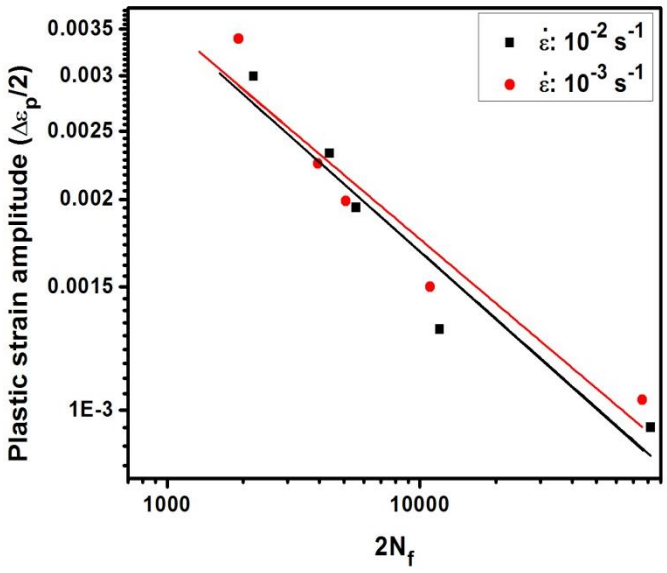

Fig. 7.3 Coffin–Manson plot of modified 9Cr–1Mo steel in normalized and tempered condition at 600 °C at strain rates of 10^{-2} s^{-1} & 10^{-3} s^{-1}.

Table 7.1 LCF parameters of modified 9Cr-1Mo steel at 600 °C.

Strain Rate (s^{-1})	**Fatigue Ductility Coefficient (ε_f')**	**Fatigue Ductility Exponent (c)**
10^{-3}	0.029	-0.304
10^{-2}	0.032	-0.319

7.4 Deformation Behavior

Cyclic deformation at 600 °C caused microstructural changes and led to development of low energy cell structure irrespective of strain amplitudes and strain rates. Figure 7.4 & 7.5 display formation of cell structure for different strain amplitudes at strain rate of 10^{-2} s^{-1} & 10^{-3} s^{-1} respectively. It is obvious from these figures that cell size increases with increase in strain amplitude at both strain rates of 10^{-2} s^{-1} & 10^{-3} s^{-1}. Coarsening of carbides is also seen in the specimens fatigue tested at 600 °C in comparison to that of the untested one (Fig. 3.1c).

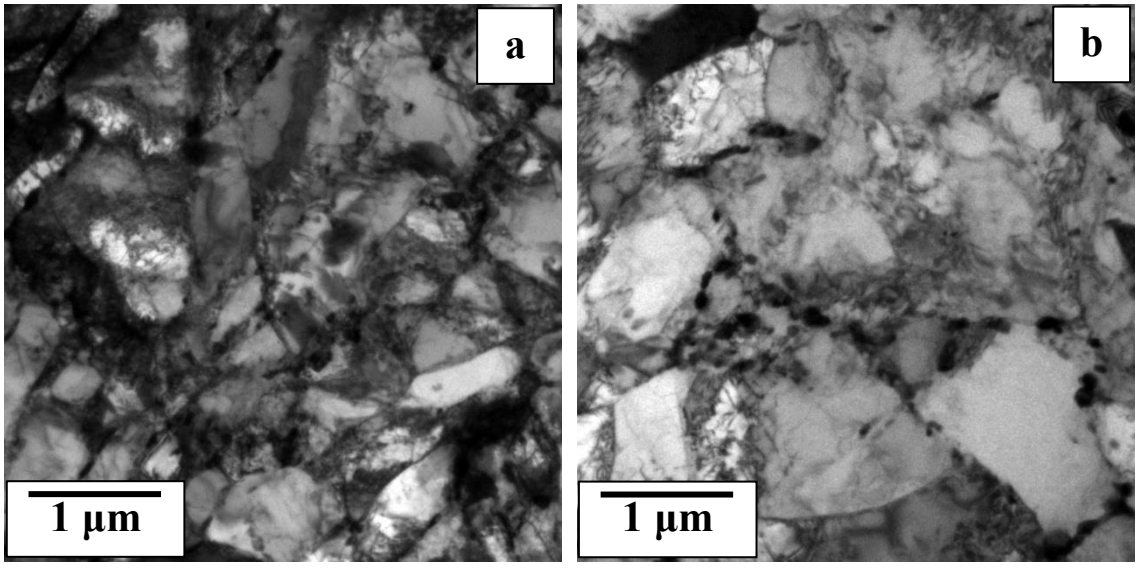

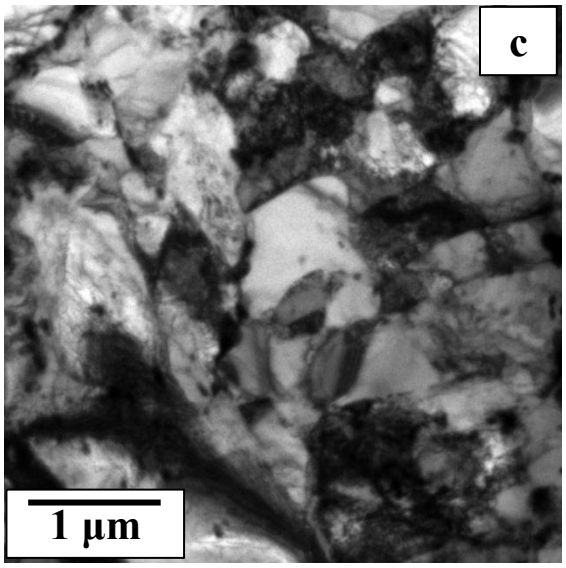

Fig. 7.4 Bright field TEM micrographs of the modified 9Cr–1Mo steel fatigue tested at strain rate of 10^{-2} s^{-1} at different strain amplitudes: (a) ±0.25%, (b) ±0.375 & (c) ±0.50%.

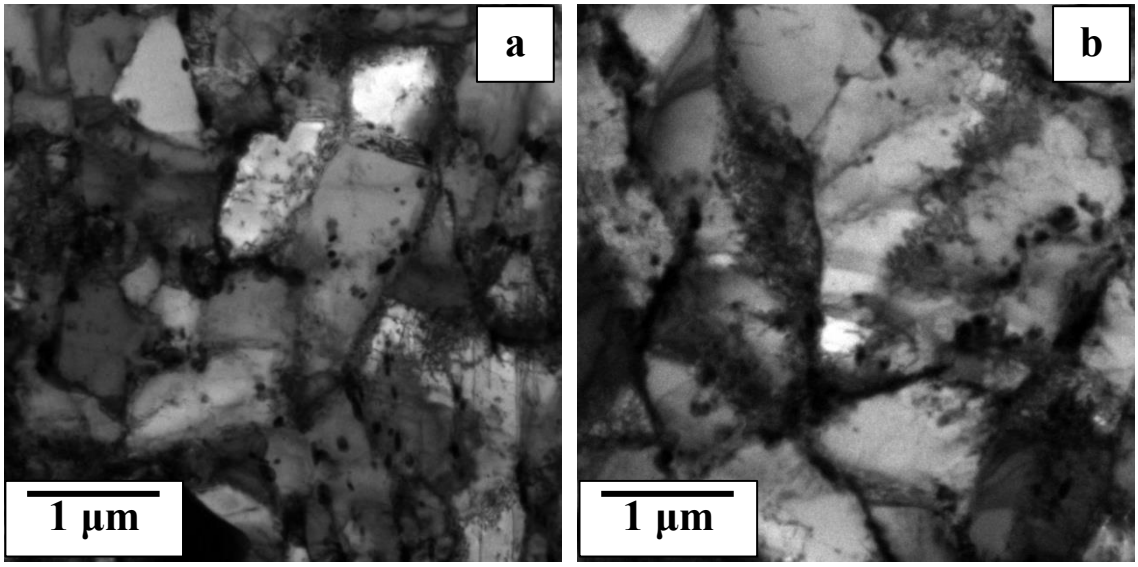

Fig. 7.5 Bright field TEM micrographs of the modified 9Cr–1Mo steel fatigue tested at strain rate of 10^{-3} s^{-1} at different strain amplitudes: (a) ±0.375 & (b) ±0.50%.

Deformation behavior of the specimens tested at different strain amplitudes at strain rate of 10^{-2} s^{-1} is also shown in Fig. 7.6. The prior austenite grain size in this steel was ≈ 20 µm. Dynamic recrystallization may be seen in the specimen tested at strain

amplitude of ±0.375% (Fig. 7.6a). Formation of subgrain and dynamic recovery is evident from Fig. 7.6b.

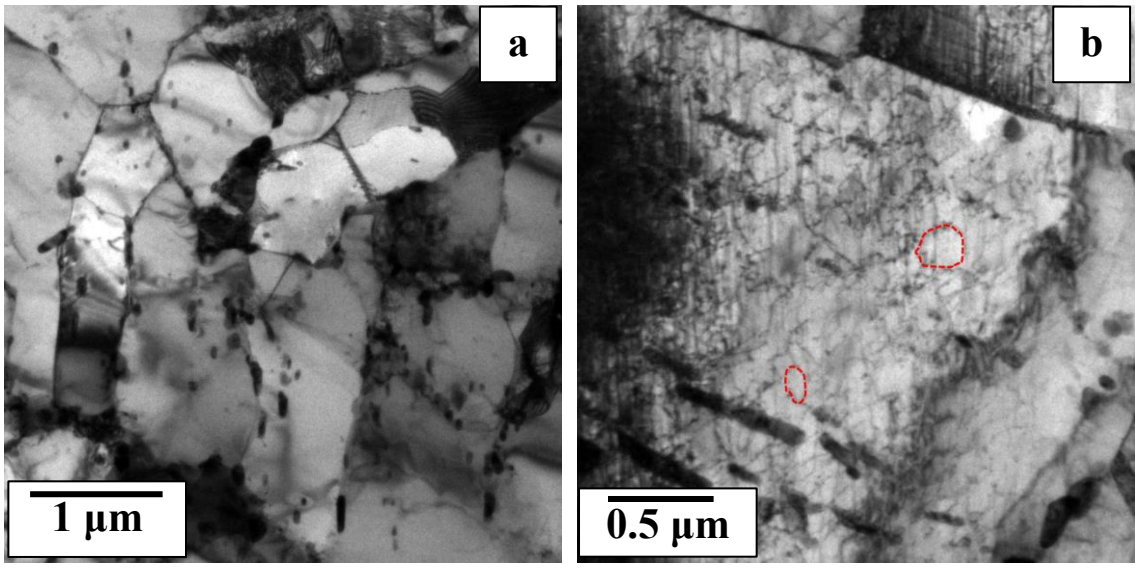

Fig. 7.6 Deformation behavior of fatigue specimens of modified 9Cr–1Mo steel tested at a strain rate of 10^{-2} s^{-1} at different strain amplitudes: (a) ±0.375%, showing dynamic recrystallization, (b) ±0.42% showing formation of sub–grain and dynamic recovery.

The dislocation structure is found to be highly heterogeneous. In some of the tempered laths fringes were also observed. These fringes could be formed due to planar faults like twinning, stacking fault, antiphase boundary or grain rotation etc. Several examinations were carried out at different tilts and it is established that these fringes developed due to grain rotation phenomena. The bright field images with fringes and corresponding diffraction patterns are shown in Figs 7.7 & 7.8 at strain rate of 10^{-2} s^{-1} and 10^{-3} s^{-1} respectively. Spot splitting in the diffraction pattern is quite obvious and the angle between the splitted spots is found to be approximately 5–6°. The splitted spots are not the perfect mirror image hence the fringes are not developed due to twinning. Fragmentation of lath boundary is also seen from the fringes formed along the lath boundary (Fig. 7.9). Dislocation configuration inside the subgrains shows array of parallel dislocations (Fig. 7.10).

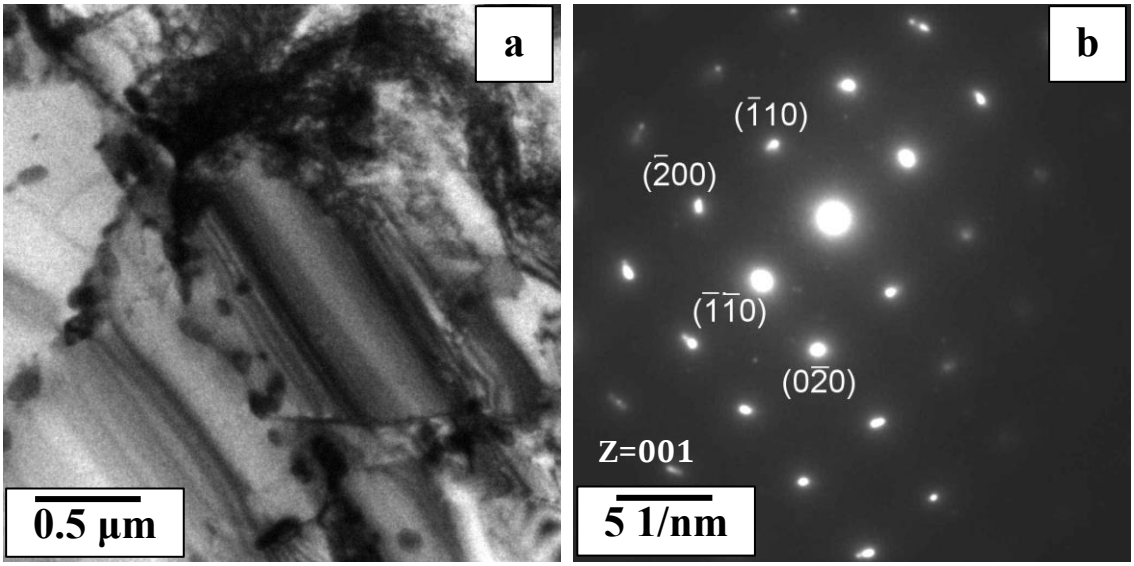

Fig. 7.7 Deformation behavior of fatigue specimen of modified 9Cr–1Mo steel tested at strain amplitude of ±0.375% at a strain rate of 10^{-2} s^{-1}: (a) bright field image showing fringes due to grain rotation, (b) corresponding diffraction pattern showing splitting of diffraction spots.

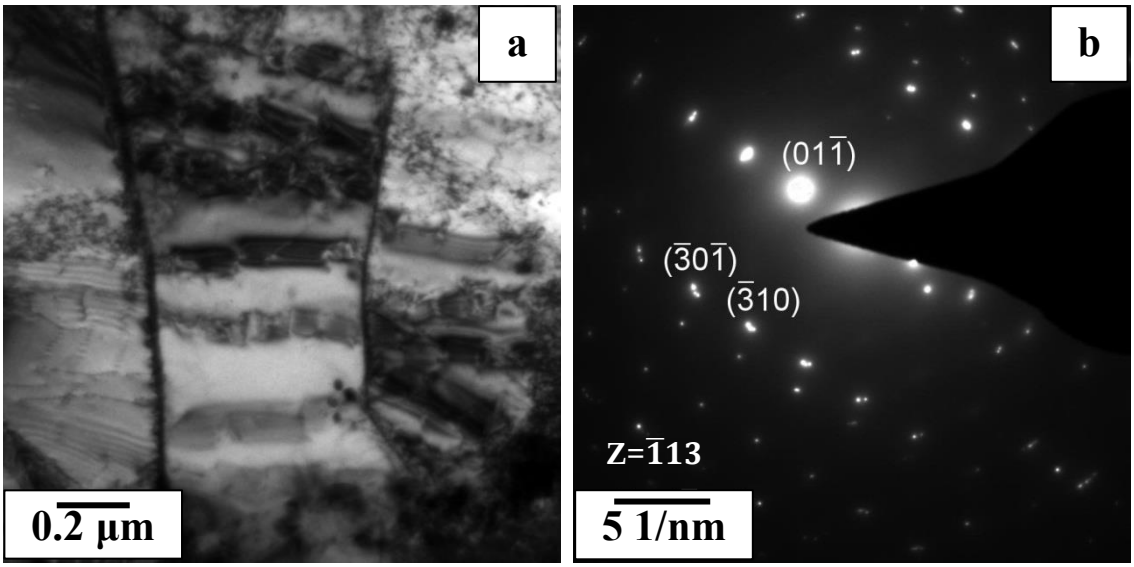

Fig. 7.8 (a) Fringes formed due to grain rotation in the specimen tested at lower strain rate of 10^{-3} s^{-1} at strain amplitude of ±0.50%, (b) splitting of the diffraction spots in the corresponding diffraction pattern.

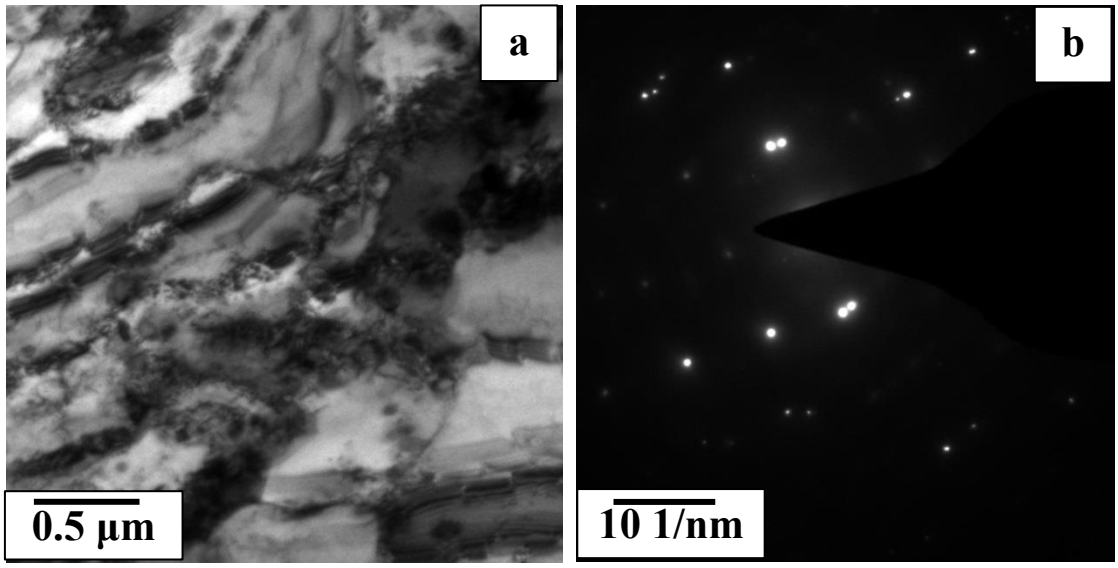

Fig. 7.9 (a) Bright field TEM micrograph showing fragmentation of lath boundaries of the specimen tested at strain amplitude of ±0.50% at strain rate of 10^{-3} s^{-1}.

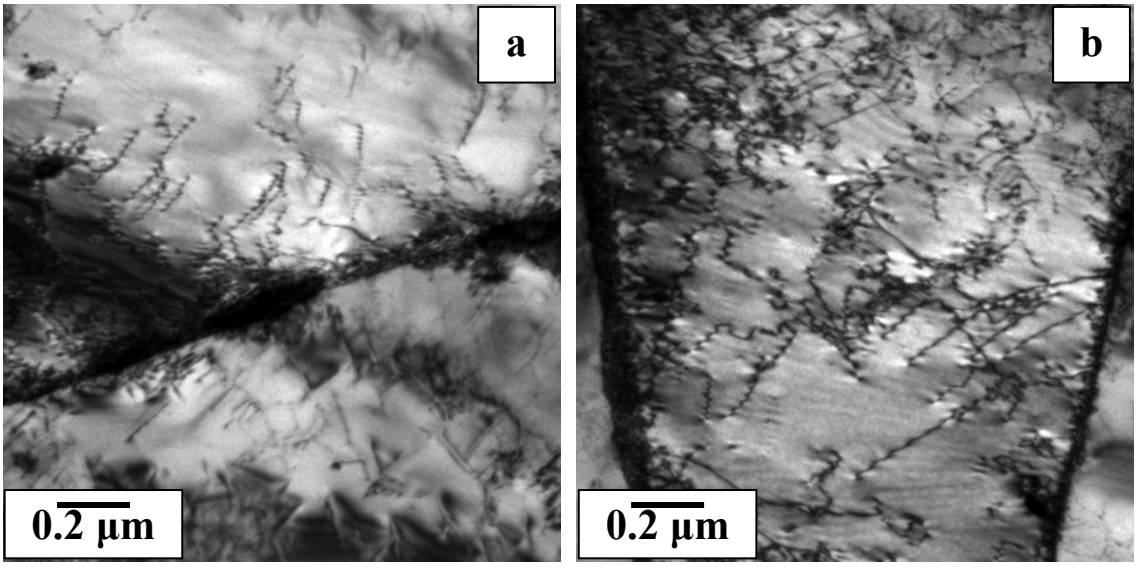

Fig. 7.10 Array of parallel dislocations in the specimen fatigue tested at strain amplitude of ±0.50% at strain rate of 10^{-3} s^{-1} at 600 °C.

7.5 Fracture Behavior

Fracture behavior of the fatigue tested specimens, at different strain amplitudes, at strain rates of 10^{-2} s^{-1} & 10^{-3} s^{-1} is shown in Figs. 7.11 and 7.12 respectively. White arrows indicate sites of fatigue crack initiation. Fatigue region is marked by white line.

Multiple crack initiation sites may be seen from the ridges along the periphery of the fracture surface. There is similar effect of strain rate and strain amplitude on the fracture behavior of the steel as at 300 °C. The length of overall fatigue crack is decreased with increase in strain amplitude at high strain rates; on the other hand there is reverse trend at lower strain rates. There is formation of multiple crack initiation sites and may be seen from the surface ridges.

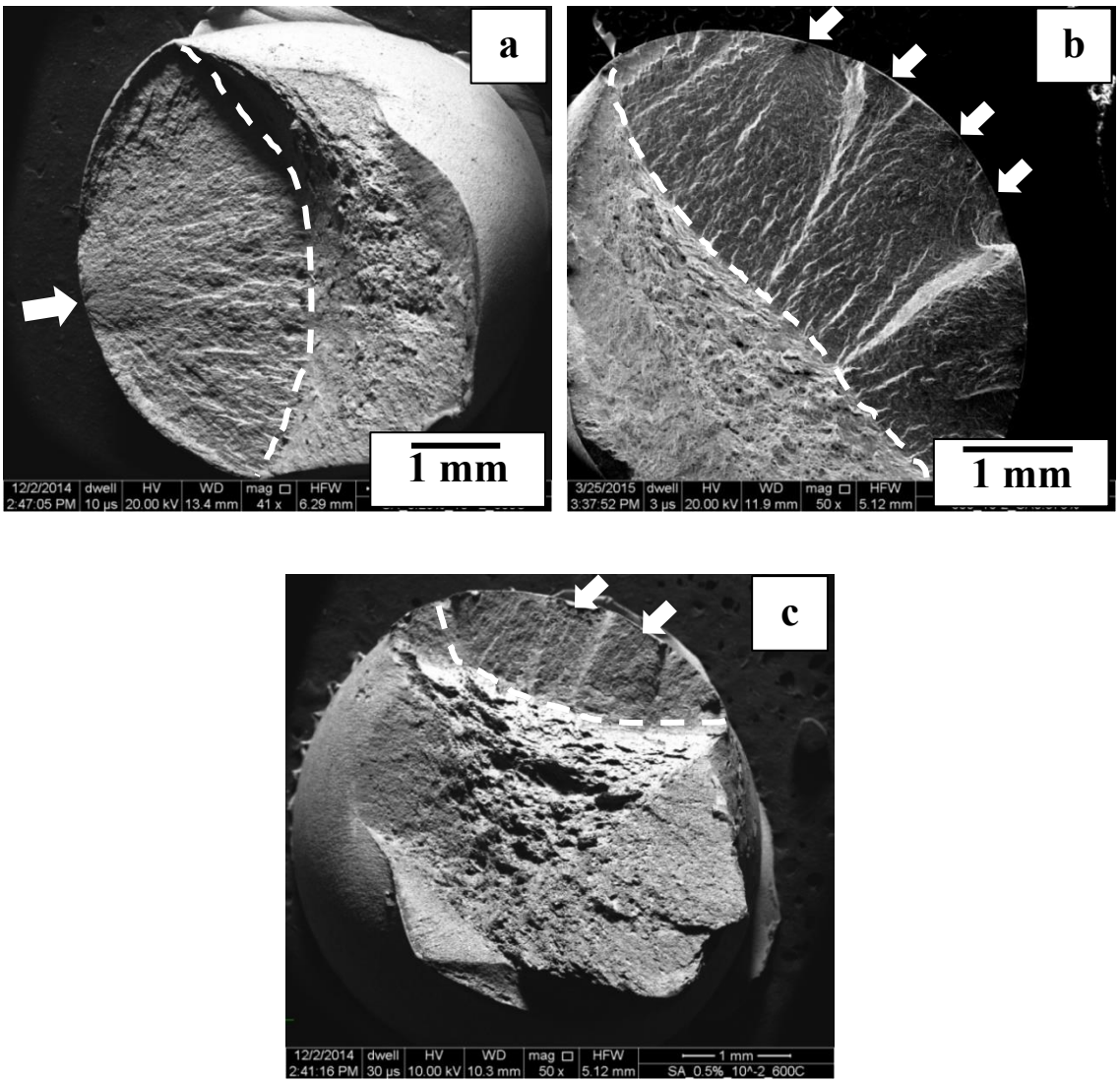

Fig. 7.11 Fracture surface of the specimens tested at strain rate of 10^{-2} s^{-1} and different strain amplitudes (a) ±0.25%, (b) ±0.375%, (c) ±0.50%.

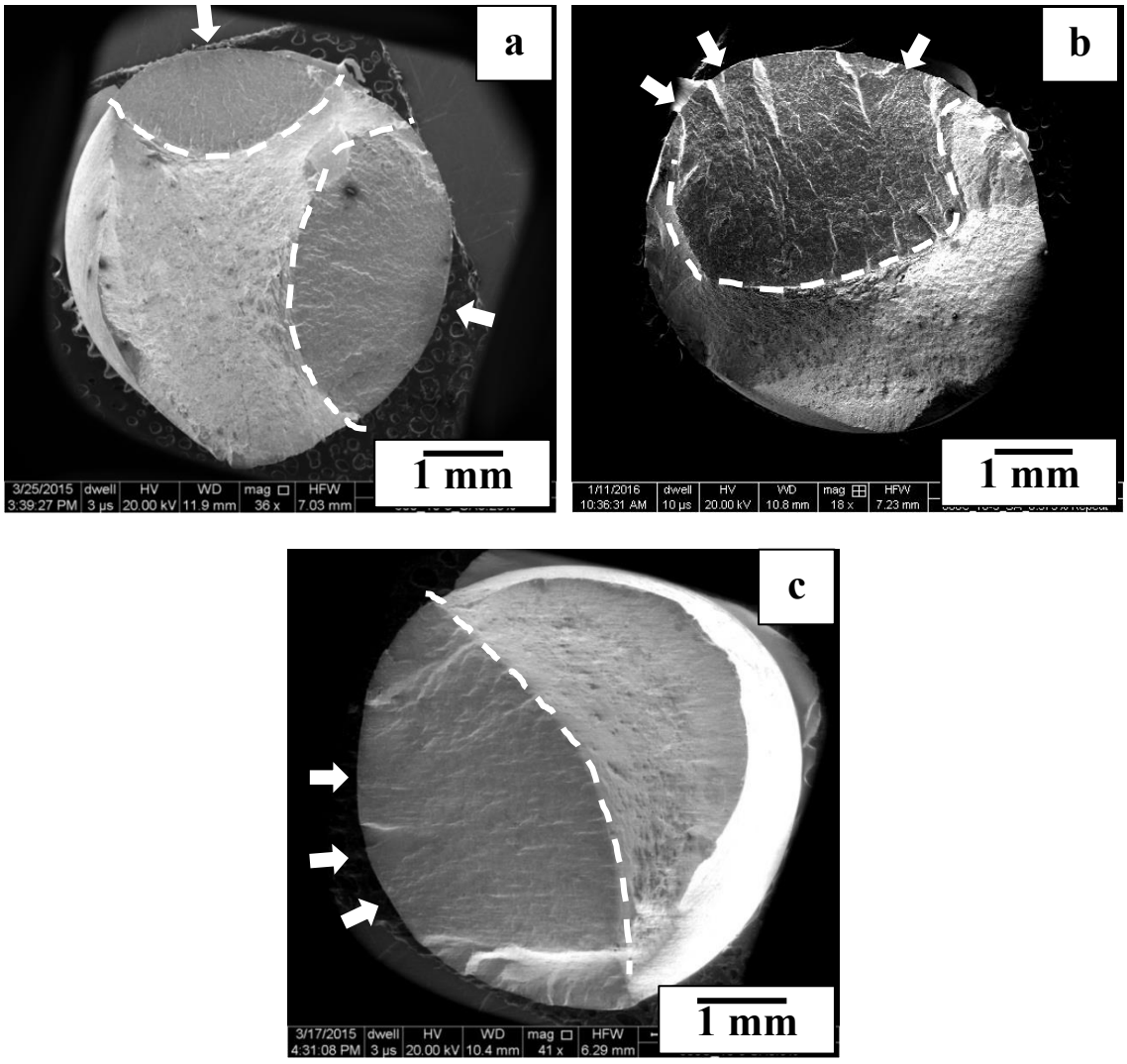

Fig. 7.12 Fracture surface of the specimens tested at strain rate of 10^{-3} s^{-1} and different strain amplitudes (a) ±0.25%, (b) ±0.375%, (c) ±0.50%.

Magnified view of the crack propagation region of fracture surfaces of the specimens fatigue tested at different strain amplitudes at strain rate of 10^{-2} s^{-1} and 10^{-3} s^{-1} is shown in Figs. 7.13 & 7.14 respectively. Inter striation spacing of stage II fatigue crack growth was evaluated from the different images and regions of the fractographs for different strain amplitudes at the both strain rates.

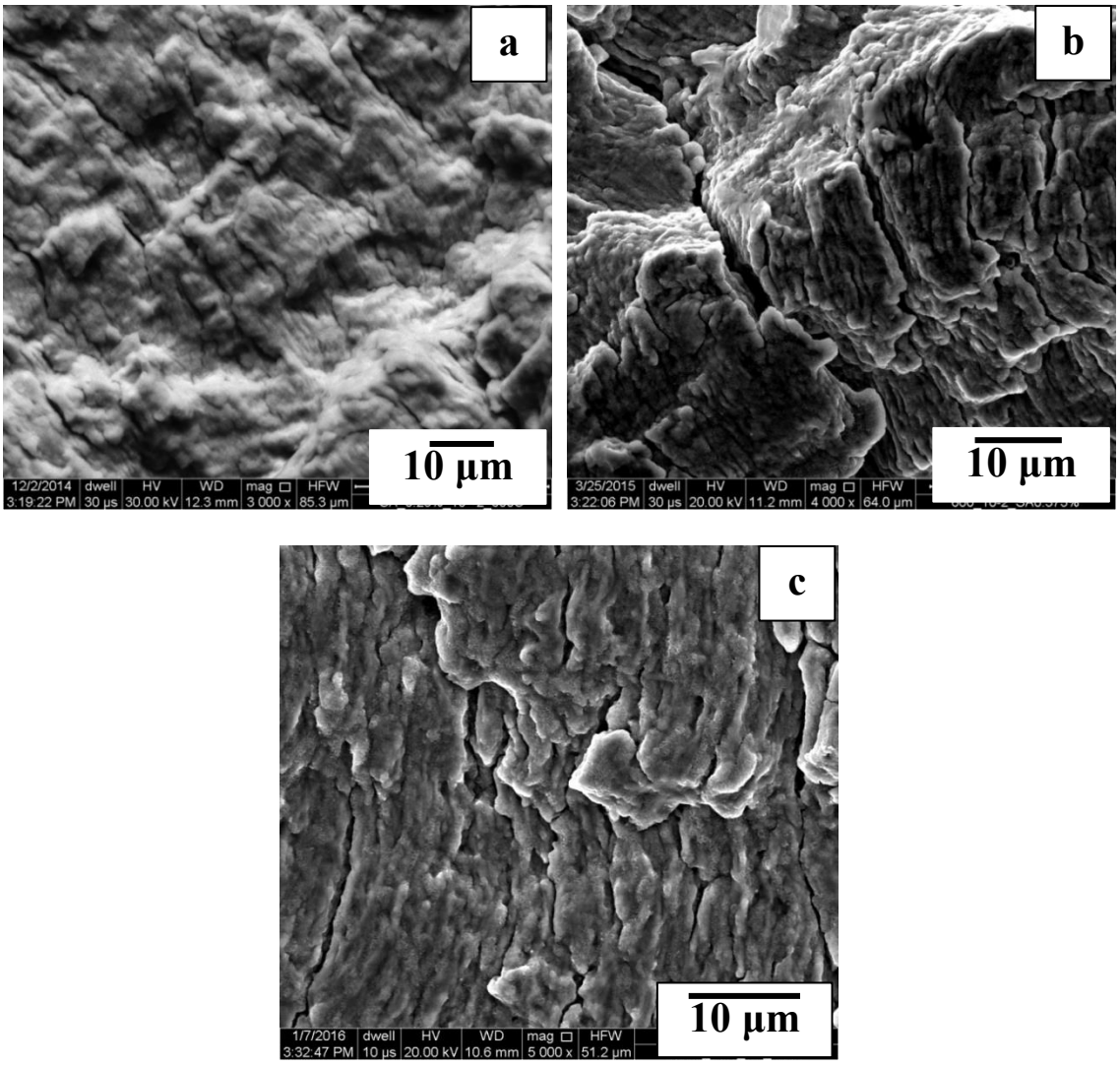

Fig. 7.13 Magnified view of the crack propagation region of fracture surface of the specimens tested at strain rate of 10^{-2} s^{-1} and at different strain amplitudes: (a) ±0.25%, (b) ±0.375%, (c) ±0.50%.

The inter striation spacing is increased with increase in strain amplitude at strain rate of 10^{-2} s^{-1} and found to be 0.7657 µm, 0.947 µm and 1.10 µm for strain amplitudes ±0.25%, ±0.375% and ±0.50% respectively. Similarly there is increase in inter striation spacing at strain rate of 10^{-3} s^{-1}. The interspacing at strain amplitude of ±0.25%, ±0.375 and ±0.50% are found to be 1.125 µm, 1.324 µm and 1.65 µm respectively. Thus, the rate of the fatigue crack growth has been increased with decrease in strain rate.

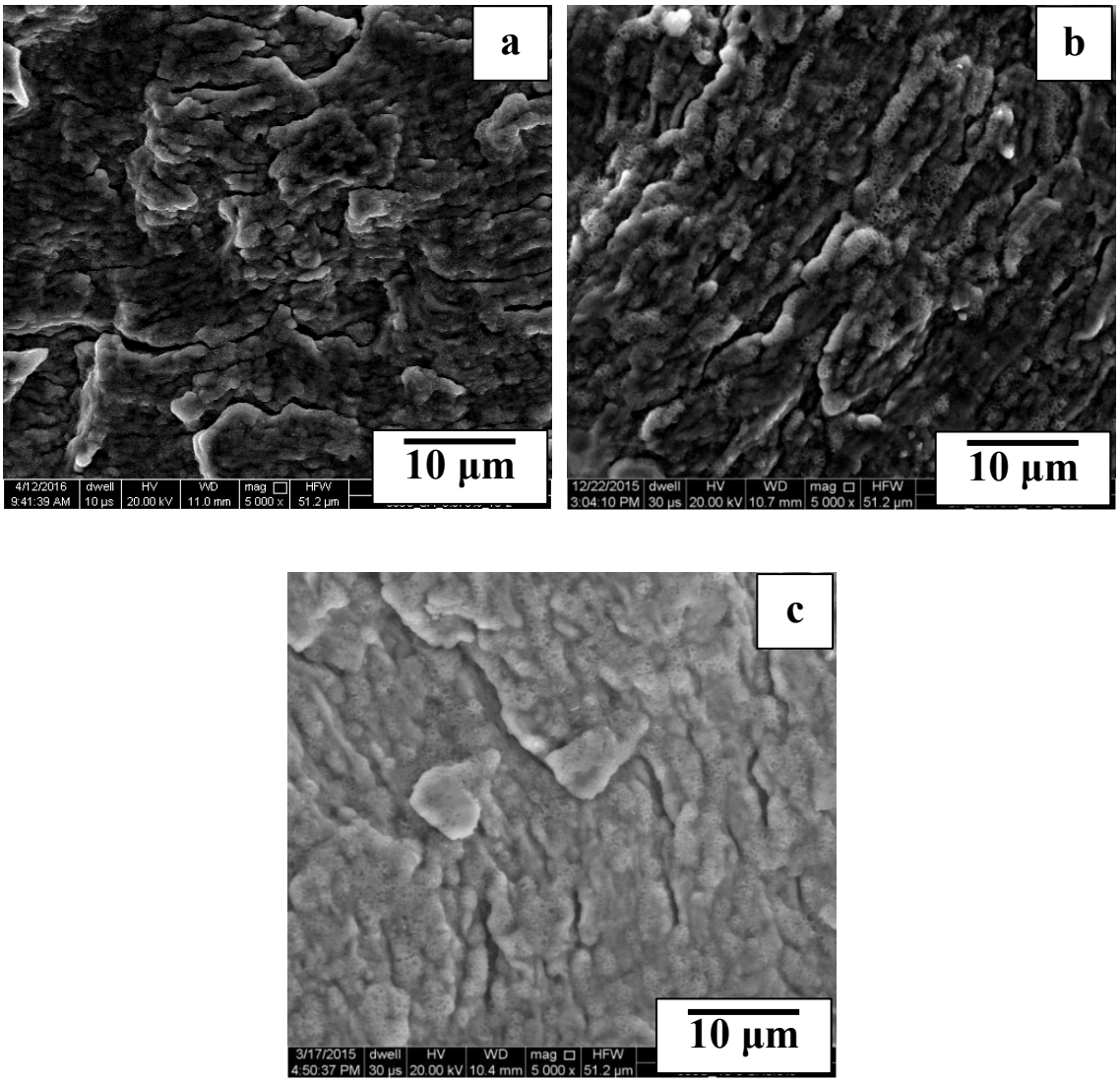

Fig. 7.14 Magnified view of the crack propagation region of fracture surface of the specimens tested at strain rate of 10^{-3} s^{-1} and at strain different amplitudes: (a) ±0.25%, (b) ±0.375%, (c) ±0.50%.

It is important to mention that there is oxidation of the steel at the test temperature of 600 °C at all the strain amplitudes and strain rates. The magnified view of the regions of fatigue crack initiation is shown in Fig. 7.15a. The severe oxidation induced cracking is evident on the fracture surface. The EDS profile of the fractured surface is shown in Fig. 7.15b which confirms the formation of oxides of Fe and Cr. The severity of surface oxidation is increased with lowering of strain amplitude and the strain rate.

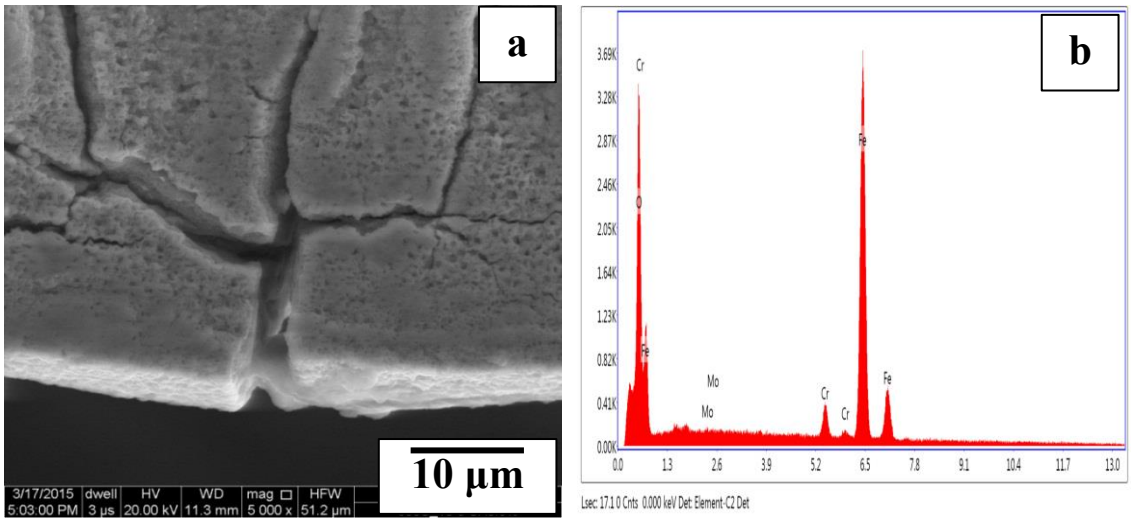

Fig. 7.15. (a) Oxidation induced cracking on the fracture surface of the fatigue specimen tested at strain amplitude of ±0.50% at strain rate of 10^{-3} s^{-1}, (b) corresponding EDS.

7.6 Discussion

Irrespective of the strain amplitude, strain rate and temperature the modified 9Cr–1Mo steel is found to exhibit cyclic softening not only at RT, 300 °C but also at 600 °C and with higher rate of softening than those at RT & 300 °C. Also the rate of softening is independent of strain rate but it is found to increase with increase in strain amplitude[62][62][62]. These observations are in line with the earlier investigation [64]. It may be seen from the dislocation structure following fatigue failure at different strain amplitudes at both strain rates (Figs 7.4 & 7.5) that there is transformation of lath marteniste structure in to equiaxed dislocation cell structure. During fatigue deformation, dislocations undergo shuttling motion and get rearranged into a lower energy configuration such as cells by cross–slip [65,69,140,166,167]. It is important to mention that in addition to this microstructural transformation, dynamic recovery/recrystallization (Fig. 7.6) and grain rotation (Figs. 7.7 & 7.8) was also observed at all the strain rates and strain amplitudes. There is also coarsening of carbides and significant decrease in dislocation density resulting from annihilation of

dislocations. It is important to mention that cyclic softening at RT and 300 °C is mainly due to rearrangement of dislocations to low energy configuration of dislocations as cells (sub–grains) structure, reduction in friction stress. In contrast to cyclic softening at RT and 300 °C in this steel, cyclic softening at 600 °C is not only due to the rearrangement of dislocations and annihilation of dislocations but also from the recovery/recrystallization, extensive grain rotation and coarsening of precipitates.

Cyclic softening in the Cr–Mo steels in literature has been reported in terms of: (i) annihilation of dislocations introduced during martensitic transformation, (ii) change of original lath structure to cells or equi–axed subgrains, (iii) degradation of strength due to coarsening of precipitates (iv) replacement of Mo–C pairs by Mo–C–Mo clusters with an associated loss in interaction solid solution strengthening and (v) complete dissolution of precipiates in the matrix [10,24,25]. Also stress reduction associated with surface oxide film formation during deformation, and low angle lath boundary elimination during cyclic softening is related to increase in lath width [4, 16,31,42].

The contributions of the different phenomena to cyclic stress response in the present work in modified 9Cr–1Mo steel are described below:

Dynamic Recovery/Recrystallization: It is well reported phenomena in materials with high density of precipitate particles, finer grain size and high dislocation density at high temperatures and high strain regime including the modified 9Cr–1Mo steels. It is also reported that pre–ageing of modified 9Cr–1Mo steels also promotes dynamic recrystallization under combined creep–fatigue deformation [40]. Dynamic recovery is commonly understood to result from reaction between mobile dislocations and segments of the stored ones [169] to reduce the stored energy but contribute to production of a viable nucleus for recrystallization in the form of well–defined subgrains. Dynamic

recovery and a critical strain are preconditions required for the occurrence of dynamic recrystallization. The process of dynamic recovery (red encircled region) is shown in Fig. 7.6b in the specimen fatigue tested at strain amplitude of ±0.42%. Dynamic recrystallization proceeds earlier and more rapidly at high temperature and high strain where the grain boundaries are more mobile in comparison to that at low temperature and low strain even though the driving force is the same [170,171]. It has also been reported that dynamic recrystallization is a possible mechanism for the grain coarsening as well as to some extent for the cyclic softening in ultrafine grained copper [172].

The microstructural modification in terms of recovery and recrystallization in the modified 9Cr–1Mo steel after post weld heat treatment was studied at different temperatures (730 & 760 °C) and for different durations (2 h & 4 h). It was observed that $M_{23}C_6$ precipitates played major role for the occurrence of recrystallization and coarsening of precipitates. The high density of dislocation around $M_{23}C_6$ with higher distortional energy results in instability of the metastable structure and this would be in advantageous position to promote recrystallization [173]. On the other hand, Nb addition in HSLA steels retarded dynamic recrystallization but Nb(C, N) precipitates hardly influenced the dynamically recrystallized grain size [174]. During the process of this type of refinement in grain size, the nucleation site areas were also increased for dynamic recrystallization and this may give rise to drastic reduction in flow stress. In the present investigation recrystallized grains are formed due to coarsening of carbide particles and high strain amplitude combined with fine subgrain structure formation at 600 °C which drastically decreased the stress during cyclic deformation.

Grain Rotation: It is also an important phenomenon occurring during high temperature deformation and recrystallization of polycrystalline materials. It is important to mention that grain rotation was observed by the authors for the first time in the modified

9Cr–1Mo steel, from cyclic deformation at 600 °C. It is believed that this also contributed to cyclic stress response of the steel. Processes for grain rotation include intra–grain dislocation processes (cross–grain glide of a large number of dislocations that re–orient the grains with respect to surrounding grains), diffusive mechanisms, as well as sliding at the grain boundaries. Grain rotation is also more obvious in fine grain size [175]. Grain rotation associated cyclic softening was reported in Zircalloy–4 where decrease in friction stress with cumulative plastic strain would activate several prism slip systems to induce grain rotation under cyclic loading. However, as the cumulative plastic strain increases, grains keep rotating (decrease of friction stress) due to an irreversible deformation increasing the interaction between dislocations. Eventually the increased internal stress by dislocation substructure increases the back stress (decreasing the irreversible deformation, making it more difficult for the grains to rotate). Grain rotation resulting in cyclic softening requires only a small amount of an irreversible deformation [176]. In connection to this it was also observed that both friction stress and back stress were found to decrease with number of cycles which further confirmed grain rotation phenomena as dominating phenomena at this temperature (Fig.7.16).

Coarsening of Carbides: Bright field TEM micrograph of this steel in normalized and tempered condition showed distribution of carbides particles (Fig. 3.1c). Coarsening of carbide particles in the fatigue tested speccimens may be clearly seen in Figs. 7.4–7.5 and quantitative values are given in Table 7.2. This also supports the cyclic softening in the material. These results are in good agreement with the earlier investigation [81,140]. It was also stated that coarsening was expected to promote the breakdown of lath structure and evolving a cell structure [80].

Table 7.2: Size of the carbides in the untested and after fatigue deformation at 600 °C

Condition	**Untested**	**LCF Tested at 600 °C**
Average size of the carbides	≈4 μm	≈13μm

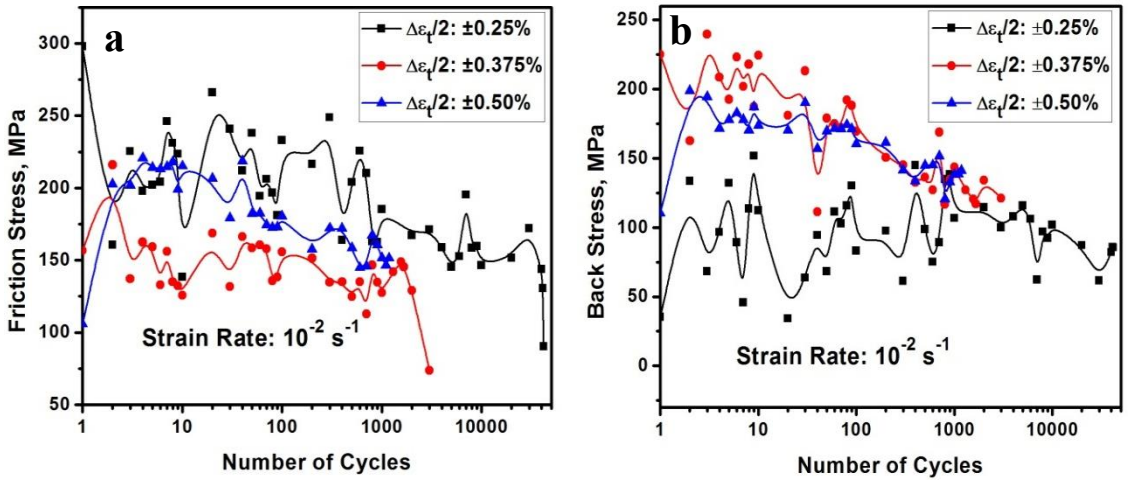

Fig. 7.16. Variation of friction stress and back stress with number of cycles for different strain amplitudes at strain rate of 10^{-2} s^{-1} at 600 °C: (a) friction stress (b) back stress.

Dislocation Annihilation: Dislocation configuration inside the grain in the fatigue tested specimen at strain amplitude of ±0.50% at strain rate of 10^{-3} s^{-1} is shown in Fig. 7.10. Array of dislocations can clearly be seen. It is essential to mention that each dislocation is having positive and negative strain field and can be clearly visualized from the schematic shown in Fig. 7.17. The positive and negative strain fields of different dislocations coincided and led to annihilation of dislocation to results in cyclic softening. Annihilation occurs between dislocations of opposite sign and critical distance is required for this. This distance depends on the type of dislocation i.e. edge or screw, crystallographic system (BCC, FCC etc.) and temperature.

The higher rate of softening at 600 °C in comparison to that at low temperature may be attributed to large extent of recovery. The process of recovery includes coarsening of carbides, grain rotation and drastic reduction in dislocation density. The rate of softening was independent of external environment.

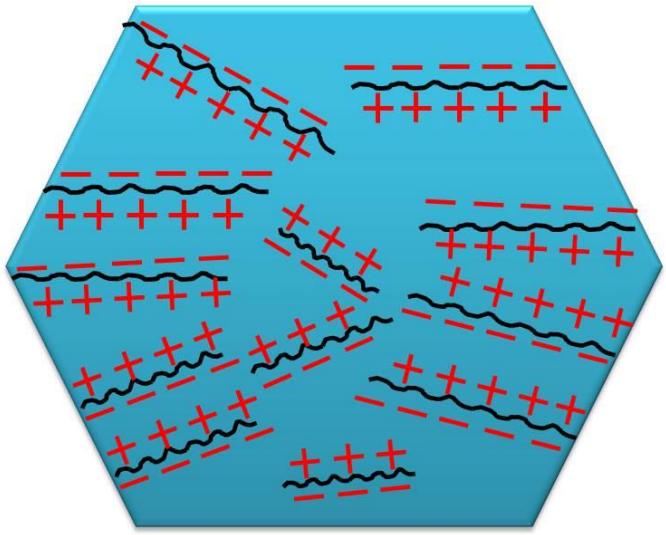

Fig. 7.17 Schematic showing annihilation of dislocations.

Fatigue failure at 600 °C is influenced by oxidation at all the strain amplitudes and at both the strain rates and it was confirmed by SEM and EDAX analysis (Fig. 7.13–7.15). Thus, reduction in fatigue life at 600 °C is considered to be affected by the environmental interaction i.e. oxidation. The role of oxidation in reduction of fatigue life has been earlier confirmed by conducting test in vacuum to result in significant increase in fatigue life [66,71]. The oxide layer formed on the surface can be easily overcome by slip. Both crack initiation and crack propagation was assisted by oxidation. The presence of external stresses (thermal or mechanical) leads either to cracking or detachment of oxide layer (spalling) that exposes fresh material to the environment. Effect of strain rate on fatigue life is shown in Fig. 7.2. It may be seen that and fatigue life is decreased at the low strain rate in comparison to that at the higher strain rate of 10^{-3} s^{-1} in comparison to that of 10^{-2} s^{-1}. The reduction in fatigue life at low strain rate may be associated with increase in the severity of oxidation. At lower strain rate more time is available for the environmental interaction of specimen exposed for longer duration at the same strain amplitude in comparison to that at the higher strain rate. This

results in higher degree of oxidation and increase in inter striation spacing at the strain rate of 10^{-3} s^{-1} in comparison to that at 10^{-2} s^{-1}. Multiple crack initiation cites were observed at the high strain amplitude.

Slip reversals and segregation of nonmetallic elements at grain boundaries can be affected by the oxidation of slip step and it may change near surface deformation behavior and mechanical properties such as fatigue crack initiation and propagation. Once the oxide layer is cracked, a fresh metallic surface directly comes in contact of the environment and oxidation starts by penetration of oxygen along the fast diffusion paths (microstructural boundaries)[166]. These cracks of the oxide layer induce stress concentration at their tips in the material. Therefore, it is easier for these cracks to propagate inside the material from these high–stress regions. Thus, the drastic reduction in fatigue life of the modified 9Cr–1Mo steel in normalized and tempered condition at 600 °C is mainly affected by the oxidation and subsequent rapid propagation of crack in a brittle manner.

7.7 Conclusions

The following conclusions may be drawn from this chapter:

- Cyclic softening is observed at all the strain amplitudes at both the strain rates, except at very low strain amplitude where there is initial stabilized stress response.
- There is increase in cyclic stress response with increase in strain rate.
- Cyclic softening at 600 °C is contributed by many factors such as cell formation, dynamic recovery/recrystallization, grain rotation, annihilation of dislocation and coarsening of carbides.

- Oxidation of the steel is observed at all the strain amplitudes and strain rates studied. The significant decrease in fatigue life at low strain rate may be due to exposure of the specimen for long duration in comparison to that at high strain rate.